Hindawi Publishing Corporation
Journal of Nanomaterials
Volume 2007, Article ID 34527, 11 pages
doi:10.1155/2007/34527

Research Article

On the Dielectric and Magnetic Properties of Nanocomposites

B. Hallouet,[1] B. Wetzel,[2] and R. Pelster[1]

[1] *Fachrichtung 7.2, Experimentalphysik, Universität des Saarlandes, Postfach 151150, 66041 Saarbrücken, Germany*
[2] *Institut für Verbundwerkstoffe GmbH (IVW), Erwin-Schrödinger-Straße, Gebäude 58, 67663 Kaiserslautern, Germany*

Received 15 February 2007; Revised 29 June 2007; Accepted 17 October 2007

Recommended by C. Brosseau

We investigate nanocomposites, that is, dispersions of magnetite nanoparticles in an epoxy resin, by means of broadband dielectric and magnetic spectroscopy. The molecular dynamics of the polymer matrix is altered by the nanoparticles. Due to the formation of agglomerates neither permittivity nor permeability can be described with known effective medium models. We use the spectral representation (Bergman theorem) to show that a model-free evaluation of the low-frequency permeability of the nanoparticles can be achieved by combining dielectric and magnetic data. In addition, the ferromagnetic resonance is studied experimentally. It occurs near 3 GHz and is independent of the particle concentration.

1. INTRODUCTION

Composite materials, consisting of magnetic nanoparticles dispersed in a polymer matrix, offer the possibility to combine the properties of their components. On the one hand, the processability and mechanical quality of the matrix is an advantage compared to ferrites. On the other hand, despite a restricted particle concentration, a sufficiently high permeability has to be achieved, especially in the high frequency range around 1 GHz. For these reasons, such composites are extensively studied, both experimentally and theoretically [1–3]. Applications are possible in various areas (magnetic sensors and transducers, electromagnetic impedance matching, microwave heating, etc.).

A composite can be considered as a so-called effective medium with homogeneous material properties (effective permittivity ε_{eff} and effective permeability μ_{eff}) as long as the wavelength of an applied electric field E and a magnetic field H is large compared to the length scale of its structural inhomogeneities, that is, large compared to particle diameters and interparticle distances. Then the measured effective material parameters are defined in terms of volume averaged fields, $\langle \varepsilon_{\text{eff}} E(r)\rangle = \langle \varepsilon(r)E(r)\rangle$ and $\langle \mu_{\text{eff}} H(r)\rangle = \langle \mu(r)H(r)\rangle$, respectively. Here, the brackets denote the volume average, $\langle \cdots \rangle = 1/V \cdot \int ... dV$, and $\varepsilon(r)$ and $\mu(r)$ the local material parameters. (This is a linear analysis where the electromagnetic response of the material does not depend on the field strengths). Performing the average for each component, these definitions read [4, 5]

$$\varepsilon_{\text{eff}} = \frac{(1-f)\varepsilon_m \langle E\rangle_m + f\varepsilon_p \langle E\rangle_p}{(1-f)\langle E\rangle_m + f\langle E\rangle_p}, \tag{1}$$

$$\mu_{\text{eff}} = \frac{(1-f)\mu_m \langle H\rangle_m + f\mu_p \langle H\rangle_p}{(1-f)\langle H\rangle_m + f\langle H\rangle_p}, \tag{2}$$

where $\langle \cdots \rangle_i$ denotes the volume average in matrix ($i = m$) and particles ($i = p$) with corresponding material parameters ε_i and μ_i. $f = V_p/V$ is the volume filling factor of the dispersed particles. The above equations illustrate two main features.

(i) The effective material parameters do not depend only on the properties of the components and their mixing ratio. The microstructure, in our case, shape and size distribution of particles as well as their spatial arrangement, directly influences the field distribution and thus ε_{eff} and μ_{eff}. Therefore, analytical exact mixture rules are only available for rather simple geometries (for monodisperse arrays of spheres and spheroids, see, e.g., [6–9]). But of course, computer simulations of two and three dimensional systems allow calculation of the effective material parameters for various particle arrangements and shapes (see, e.g., [10–18]). For example, Fu et al. have found an analytically exact solution in 3D space, a complex set of equations, describing an arbitrary distribution of nontouching spheres [19]. For a given particle

Table 1: Properties of the components.

Component	DER332	DETA	Fe_3O_4
Producer	DOW	DOW	Sigma-Aldrich
State (298.15 K/343.15 K)	Crystalline/liquid	Liquid	Powder
Density (g/cm^3)	1.16	0.9482	5.1

arrangement, this allows numerical calculation of the effective permittivity [20]. Such simulations of effective properties are helpful, but they do not resolve the problem of how to analyze experimental data, when the microstructure is not completely known, for example, due to a partial agglomeration of particles. There is a multiplicity of approximate effective-medium formulas [21, 22], but in most cases, the details of the underlying microstructure are not explicitly specified. Thus it is often not clear how to chose the one that is appropriate for the system under study. Especially the attempt to evaluate the properties of the dispersed component is impossible or, at least, subject to big errors (note that heterogeneity not only affects the absolute values of effective permittivity but also influences the characteristic frequencies of polarization processes [23] and of molecular relaxation dynamics [24], that are observable in dielectric spectroscopy).

(ii) For a given microstructure, the same formal relationship holds for permittivity and permeability: (1) transforms into (2), when E is replaced by H as well as ε by μ. Since the fields behave in an analogous way at the internal interfaces (the tangential components E_t and H_t are continuous whereas for the normal components, $\varepsilon_p E_{\perp,p} = \varepsilon_m E_{\perp,m}$ and $\mu_p H_{\perp,p} = \mu_m H_{\perp,m}$ hold), the same mixture rules apply for ε_{eff} and μ_{eff}.

For the effective permittivity, there exists a so-called spectral representation, that was developed by Bergman, Fuchs, and Milton (for a review see [25]). They were able to separate the influence of microstructure, characterized by a spectral density function, from that of the components, characterized by their permittivities [25]:

$$\frac{\varepsilon_{\text{eff}}}{\varepsilon_m} = 1 + f\left\{\frac{C}{t_\varepsilon} + \int_0^1 \frac{g_f(n)}{t_\varepsilon + n}dn\right\} \quad \text{with } t_\varepsilon = \frac{1}{\varepsilon_p/\varepsilon_m - 1}. \tag{3}$$

The constant C is the strength of percolation describing the contribution of an infinite cluster. The spectral density $g_f(n) \geq 0$ characterizes the actual microstructure at a given filling factor f (for a single particle n would correspond to the depolarization factor; in a complex system of interacting particles, it is a variable in the range $0 \leq n \leq 1$). There are two sum rules that determine the 0th and the 1st moment of the function $g_f(n)$:

$$\int_0^1 g_f(n)dn = 1 - C, \tag{4}$$

for all mixtures (i.e., g_f is normalized), and additionally,

$$\int_0^1 n g_f(n)dn = \frac{1}{3}\cdot(1 - f), \tag{5}$$

for isotropic systems.[1] In the following, we restrict ourselves to isotropic composites below the percolation threshold ($C = 0$ in (3) and (4)). Due to the above formal analogy between effective permittivity and permeability, the same spectral density function also describes the magnetic properties of a composite:

$$\frac{\mu_{\text{eff}}}{\mu_m} = 1 + f\int_0^1 \frac{g_f(n)}{t_\mu + n}dn \quad \text{with } t_\mu = \frac{1}{(\mu_p/\mu_m) - 1}. \tag{6}$$

Spectral representation does not provide a method for determining $g_f(n)$ from first principles [25], and thus it does not allow derivation of mixture formulas. But it can be very helpful for the analysis of experimental data, even in cases where the microstructure is unknown. For example, when the measured effective properties vary considerably as a function of frequency, the spectral density g_f can be evaluated using model functions for the intrinsic material parameters [28–30]. In the following, we are going to show that it is possible to evaluate the material parameters of the dispersed component as well as to detect and to quantify effects that the effective medium theory does not predict (changes of the components properties at interfaces, see below). Here, we study a model system consisting of magnetic nanoparticles (magnetite) dispersed in a polymer matrix. We have measured permittivity and permeability for different particle concentrations using dielectric spectroscopy in the frequency range from 5 Hz to 1 GHz and magnetic measurements from 5 MHz to 6 GHz.

2. EXPERIMENTAL

2.1. Samples

The composites studied are an epoxide system filled with magnetic nanoparticles. This epoxide system is composed of a resin, Diglycidylether of Bisphenol A (DER332, DOW Plastics (Rheinmünster, Germany)), and a hardener, Diethylentriamin (DETA, DOW Plastics (Rheinmünster, Germany)). The magnetic nanoparticles, which have a mean diameter between 20 and 30 nm, are magnetite (Fe_3O_4) purchased from Sigma-Aldrich (Munich, Germany). The main characteristics of the components are listed in Table 1.

[1] These lower moments are obtained via a series expansion of $\varepsilon_{\text{eff}}/\varepsilon_m$ around $\varepsilon_p/\varepsilon_m = 1$, that is, considering the limiting case of a nearly homogeneous composite, where the electric field is uniform (for details, we refer to [26, 27]).

The sample preparation was done in two steps. At first, a concentrated epoxide/nanoparticle masterbatch with a particle content of 14.1 vol% was produced at the IVW (Institut für Verbundwerkstoffe). Then this masterbatch was further processed to obtain solid samples with different particle concentrations.

Nanoparticles in powders adhere to each other due to interactive forces between the particles, resulting in nanoparticle agglomerates with dimensions of several micrometers. In order to obtain a material with good mechanical properties, it is necessary to disintegrate the agglomerates and to distribute them homogeneously in the polymer matrix. In this study, two working principles, traditionally used for lacquer processing (dissolver and bead mill) were combined in one. After incorporating the powdery nanoparticles into the liquid resin, the resulting mixture was homogenized by a dissolver aggregate (a dissolver provides high shear forces by the rotation of a metal disc in the liquid mixture). Entrapped air was removed by vacuum. Then the magnetite was further dispersed using a torus mill. It applies high shear forces to the mixture via a rotating metal disc while hard zirconia beads with diameters between 1.2 and 1.7 mm move within the mixture. These beads generate collision effects and shear forces providing a grinding effect that further decreases the size of nanoparticle agglomerates. The beads were removed from the mixture after the dispersion process. The above processing of nanocomposites was performed under controlled conditions, that is, at constant energy input and constant temperature. The chosen particle content of the masterbatch (14.1 vol%) is close to the processing limit. At higher concentrations, the system becomes too viscous, resulting in an unstable and discontinuous flow during processing. Then dispersing the nanoparticles and wetting them with polymer becomes more and more difficult, and processing may result in a reduced homogeneity of the mixture.

In the next step, we have prepared solid samples with a specific particle concentration: at first, both the initial masterbatch and the pure resin were maintained for one hour under vacuum in order to remove entrapped air. This was done at a high temperature of 313.15 K to avoid crystallization and to diminish the viscosity of the resin. Then the masterbatch was diluted with pure resin whereas both components were mixed for 30 minutes and evacuated for one hour. This mixture was cured after adding the corresponding quantity of DETA (mass ratio resin/hardener 100 : 14). In this last phase, the material was mixed for five minutes, cooled down rapidly to room temperature in order to slow down the polymerization process, and evacuated for three minutes. The polymerization took place in a mould at room temperature. After 48 hours, the post-cure was performed at 393 K during one hour [31]. The resulting series of samples with varying nanoparticle content from $f = 2\%$ to $f = 10\%$ are listed in Table 2.

2.2. Measurement techniques

We have used dielectric and magnetic spectroscopy to determine the complex permittivity $\varepsilon = \varepsilon' - i\varepsilon''$ and the magnetic permeability $\mu = \mu' - i\mu''$ of our samples at room temperature.

Table 2: Volume filling factor and mass filling factor of the samples studied.

Filling factor f (% vol)	Filling factor $\times$ (% mass)
0	0
2	8.6
4	16.1
6	22.7
8	28.6
10	33.8

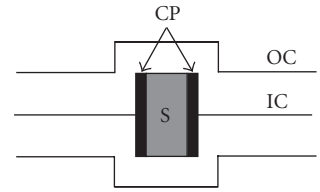

Figure 1: Condenser cell as a part of a transmission line (dielectric measurements). S: sample, CP: capacitor plates, IC/OC: inner/outer conductor of the transmission line

The complex permittivity has been measured using a broadband transmission method covering the frequency range from 5 Hz to 1 GHz with one experimental setup [32]. The sample is placed between two circular capacitor plates that are connected to the inner conductor of a coaxial transmission line (see Figure 1). For this purpose, cylindrical discs with a diameter of $\Phi = 13$ mm and a thickness d between 1 and 2 mm have been machined from the composite material (using a turning lathe). From the measured transmission coefficient, the permittivity is calculated. The respective geometrical tolerances of sample diameter and thickness ($\pm 20\,\mu$m) result in an uncertainty of $\Delta_{\text{rel}}|\varepsilon| \simeq \Delta_{\text{rel}}(\Phi^2/d) \simeq 2\%$ (for details, see [32]).

The complex permeability has been measured using an impedance analyzer (Agilent HP 8424a) in the frequency range from 5 MHz up to 110 MHz and a network analyzer (HP 8510B) between 110 MHz and 6 GHz. In both cases, the sample is inserted at the short-circuited termination of a calibrated coaxial transmission line (see Figure 2). For this purpose, cylindrical samples with outer diameter $\varphi_2 = 7$ mm and inner diameter $\varphi_1 = 3.04$ mm have been machined from the original cured composite. At low frequencies, the termination impedance of the coaxial line is measured, $Z = R + i\omega L$, with R being the resistance of the inner conductor and $L = (\mu_0/2\pi)\mu \ln(\varphi_2/\varphi_1)d$ being the inductance ($\mu_0 = 4\pi \cdot 10^{-7}$ H/m). Two measurements, with and without the sample, are sufficient to determine the complex permeability:

$$\mu = \frac{Z_{\text{sample}} - Z_{\text{empty}}}{i\omega(\mu_0/2\pi)\ln(\varphi_2/\varphi_1)d} + 1, \tag{7}$$

where ω is the circular frequency and d is the thickness of the sample [33]. The geometrical tolerances of inner and outer sample diameters ($\pm 20\,\mu$m) result in an uncertainty of $\Delta_{\text{rel}}|\mu| \simeq 2\%$.

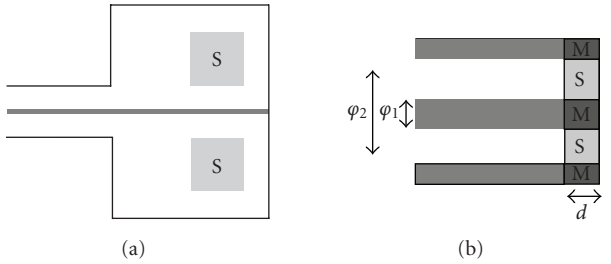

Figure 2: Measurement cell for the determination of the complex permeability in the low frequency range (a) and in the high frequency range (b) (impedance and reflection measurements, respectively). S: sample, M: metal, φ_1/φ_2: inner/outer diameter of the sample, d: thickness of the sample.

In the high frequency range, the reflection coefficient Γ is measured, which is directly connected to the measured impedance $Z = Z_{\text{sample}}$ or $Z = Z_{\text{empty}}$ and the impedance of the cable, $Z_c = 50\,\Omega$:

$$\Gamma_{\text{meas}} = \frac{Z - Z_c}{Z + Z_c}. \tag{8}$$

3. DIELECTRIC MEASUREMENTS

At room temperature, that is, below the glass transition temperature of the polymer matrix ($T_G = 404\,\text{K}$ [34]), we have performed dielectric measurements on the samples listed in Table 2. Figure 3 shows real and imaginary parts of the effective permittivity as a function of frequency for different filling factors. Already the pure matrix ($f = 0\%$) shows a relaxation process near 10^5 Hz leading to a decrease of permittivity from a low frequency value $\varepsilon_{\text{eff},s}$ to a high frequency value $\varepsilon_{\text{eff},\infty}$ above 1 GHz (Figure 4). The peak in ε'' seems to be an overlap of several processes. Local heterogeneity, for example, can give rise to such a distribution of relaxation times. The origin of this relaxation has to be clarified by further temperature dependent measurements. With increasing amount of nanoparticles, the process becomes more pronounced. In order to quantify this, we have fitted the curves with the empirical Havriliak-Negami model [35, 36]:

$$\varepsilon_{\text{eff}}(\omega) = \varepsilon_{\text{eff},\infty} + \frac{\varepsilon_{\text{eff},s} - \varepsilon_{\text{eff},\infty}}{\left(1 + (i\omega\tau)^{\alpha}\right)^{\beta}}, \tag{9}$$

with τ being the relaxation time. An example is shown in Figure 4. Although the fit does not reproduce the detailed structure of the ε''-peak, the overall agreement is good allowing at least to satisfactorily describe the respective low and high frequency limits of permittivity. The addition of nanoparticles yields both an increase of ε_∞ as well as of the relaxation strength, $\Delta\varepsilon_{\text{eff}} = \varepsilon_{\text{eff},s} - \varepsilon_{\text{eff},\infty}$ (see Figures 3 and 4). At first sight, this can be qualitatively related to the fact that the magnetite particles are conductive. When an electric field is applied, the particles become polarized, resulting in an enhanced permittivity compared to that of the pure matrix (interfacial polarization process or Maxwell-Wagner-Sillars polarization). The measured spectra thus reflect the superposition of at least two processes: the intrinsic relaxation of the polymer matrix and the polarization of the conductive particles. In the following, we will address two questions.

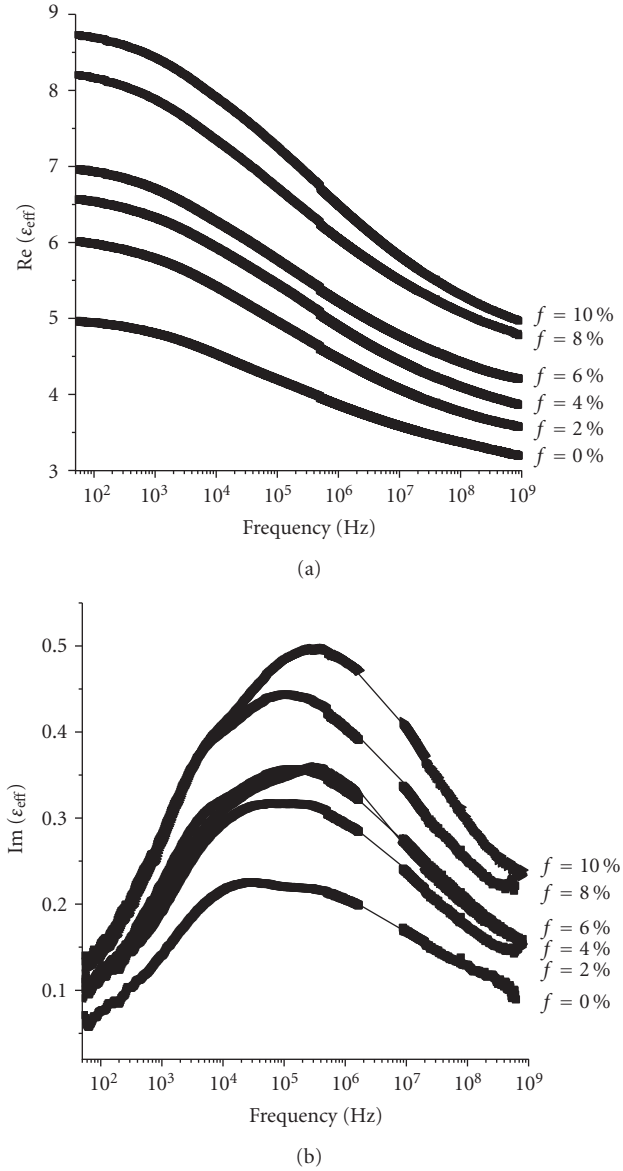

Figure 3: (a) Real and (b) imaginary parts of the dielectric function for an epoxy resin with Fe_3O_4-nanoparticles at various volume filling factors.

(i) Is the observed increase of permittivity only a simple polarization effect or do other processes, that effective medium theory do not predict, contribute?

(ii) To what extend does the data reflect the microstructure of the composite?

The spectral representation (3) is a useful tool to address the first question, even though the detailed microstructure is unknown. We thus start our discussion with a two phase system (matrix and particles) in the strict sense. Particles are either perfectly connected or well separated, so that there is no charge transfer. Additional interphases or contact resistances between particles are excluded (but we will come back to this point later).

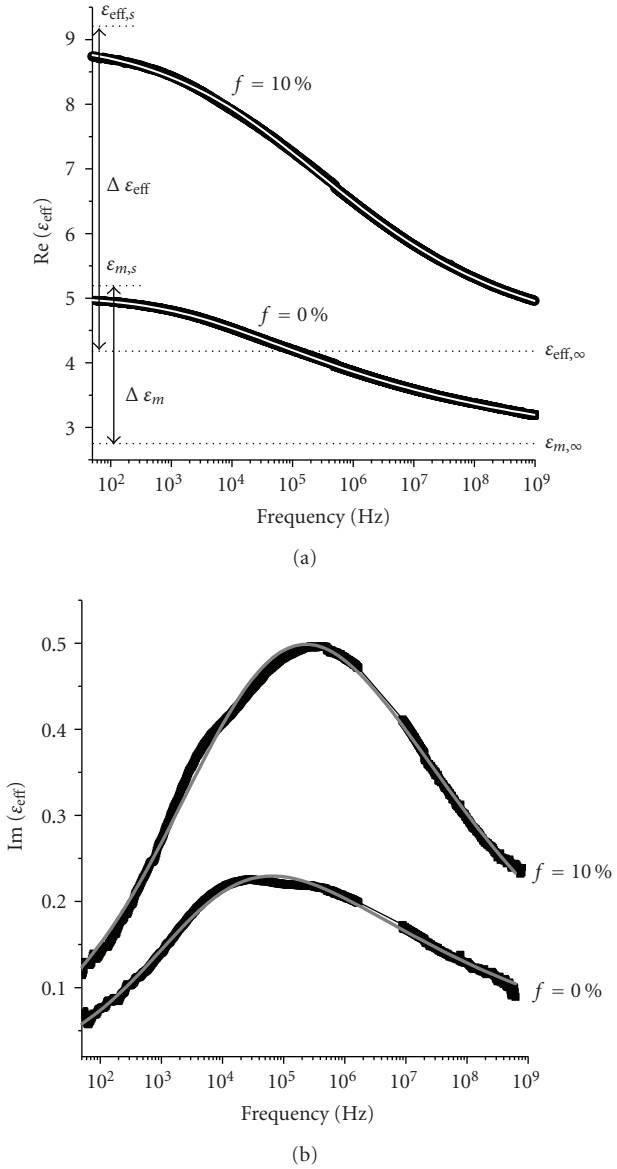

Figure 4: (a) Real and (b) imaginary parts of permittivity versus frequency for the pure polymer matrix as well as for a composite with $f = 10\%$. The thin lines correspond to (9). In (a), also some fitted parameters are shown (dotted lines): low-frequency permittivity $\varepsilon_{\text{eff},s}$ and high-frequency permittivity $\varepsilon_{\text{eff},\infty}$. The arrows indicate the respective relaxation strength, $\Delta\varepsilon_{\text{eff}} = \varepsilon_{\text{eff},s} - \varepsilon_{\text{eff},\infty}$.

The generalized permittivity of conducting particles is given by $\varepsilon_p = \varepsilon' - i\sigma/(\varepsilon_0\omega)$, so that the conductivity σ governs the dielectric response at low frequencies ($\varepsilon_0 = 8.854\cdot 10^{-12}$ F/m). When the nanoparticles are exposed to an electric field, they become completely polarized, that is, the average field strength inside is negligible compared to that outside (for a single sphere in an homogeneous field, e.g., $\langle E\rangle_p/\langle E_m\rangle = 3\varepsilon_m/(\varepsilon_p + 2\varepsilon_m)$ holds). This is the case at low frequencies when

$$\left|\frac{\varepsilon_p}{\varepsilon_m}\right| \simeq \frac{\sigma}{\varepsilon_0\varepsilon_m\omega} \gg 1, \tag{10}$$

holds, that is, in the quasistatic limit

$$\nu \ll \frac{\sigma}{2\pi\varepsilon_0\varepsilon_m} = \nu_g. \tag{11}$$

The DC conductivity of bulk magnetite is of the order of $\sigma \geq 300$ S/m at room temperature, for thin films with a thickness of 30 nm, it is $\sigma \geq 30$ S/m [37]. With a matrix permittivity $\varepsilon_m \geq 3$ (see Figure 3), the above condition reads $\nu \ll 10^{11}$ Hz. Obviously, this is the case in our measurement range (up to 10^9 Hz). Then (3) becomes, with $|t| = |\varepsilon_p/\varepsilon_m - 1|^{-1} \ll 1$,

$$\frac{\varepsilon_{\text{eff}}}{\varepsilon_m} = \underbrace{1 + f\cdot\int_0^1 \frac{g_f(n)}{n}dn}_{=h(f)} \quad \text{for } \nu \ll \nu_g, \tag{12}$$

where $h(f)$ is a function having real values $[h(f)\varepsilon R]$. Here, we have assumed that no percolation occurs ($C = 0$). In fact, our composites do not show a DC conductivity. Therefore, $\varepsilon_{\text{eff}}/\varepsilon_m = h(f) \geq 1$ holds. This ratio depends on the actual microstructure, and so it is a function of the filling factor f. But it is independent of ε_m and ε_p. As a consequence, the values of $h(f)$ do not depend on frequency and are real numbers. This is a general result that reflects in all specific mixture formulas. The Maxwell-Garnett formula, for example, that describes a random distribution of monodisperse spheres [19, 20], reads, in the quasistatic limit,

$$\frac{\varepsilon_{\text{eff}}^{\text{MG}}}{\varepsilon_m} = \frac{1+2f}{1-f} \quad \text{for } \nu \ll \nu_g, \tag{13}$$

while the Hanai-Bruggeman formula, describing randomly distributed spheres having a sufficiently broad size distribution [20], becomes

$$\frac{\varepsilon_{\text{eff}}^{\text{HB}}}{\varepsilon_m} = \frac{1}{(1-f)^3} \quad \text{for } \nu \ll \nu_g. \tag{14}$$

We have calculated the ratio of the measured permittivities, $\varepsilon_{\text{eff}}/\varepsilon_m$, and displayed its absolute value in Figure 5. Obviously, it depends on frequency in the range where the relaxation process of the matrix polymer is active (there also, the imaginary part of $\varepsilon_{\text{eff}}/\varepsilon_m$ does not vanish). This means that the observed increase of relaxation strength with filling factor (Figure 6) is not solely due to the polarization of the conductive particles. Besides the two processes we have already discussed, that is, the intrinsic relaxation of the polymer matrix and the quasistatic polarization of the conductive particles, there is an additional mechanism, that is not taken into account by effective medium theory. In order to quantify this effect, we now evaluate how the effective relaxation strength should change if there were no such additional mechanism, that is, if (12) were valid. For the respective low and high frequency values, it reads

$$\begin{aligned}\varepsilon_{\text{eff},s} &= h(f)\cdot\varepsilon_{m,s},\\ \varepsilon_{\text{eff},\infty} &= h(f)\cdot\varepsilon_{m,\infty},\end{aligned} \tag{15}$$

and thus with $\varepsilon_{\text{eff},s} = \Delta\varepsilon_{\text{eff}} + \varepsilon_{\text{eff},\infty}$ and $\varepsilon_{m,s} = \Delta\varepsilon_m + \varepsilon_{m,\infty}$ (see Figure 4),

$$\Delta\varepsilon_{\text{eff}}(f) = \varepsilon_{\text{eff},\infty}(f)\cdot\frac{\Delta\varepsilon_m}{\varepsilon_{m,\infty}}. \tag{16}$$

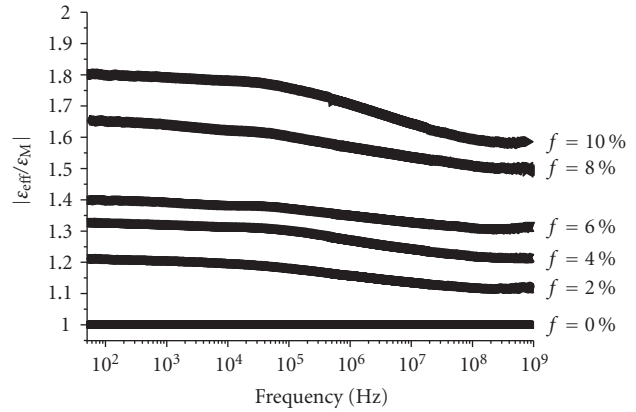

FIGURE 5: Absolute value of the ratio of effective permittivity over matrix permittivity as a function of frequency for our composites (the curves were calculated from the measured complex values shown in Figure 3). For each filling factor, effective medium theory predicts a real and frequency-independent value (see (12)). Obviously, this is not the case in the range where the relaxation of the matrix polymer is observed.

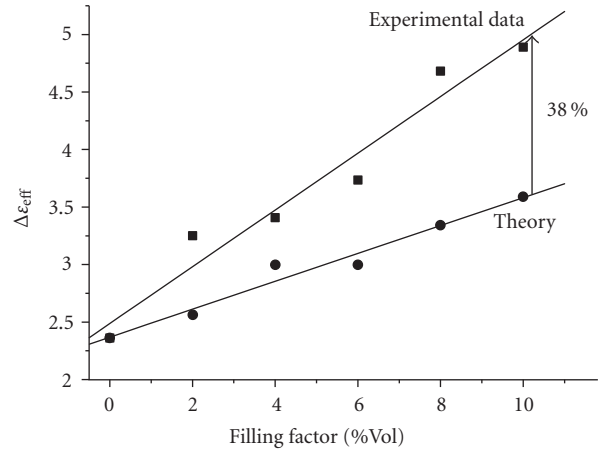

FIGURE 6: Relaxation strength $\Delta\varepsilon_{\text{eff}}$ as a function of volume filling factor. Since the relaxation process is already observed at $f = 0$, it is related to the molecular dynamics of the pure matrix. The theoretical values have been calculated using (16) (inserting the measured values $\varepsilon_{\text{eff},\infty}(f)$, $\Delta\varepsilon_m$ and $\varepsilon_{m,\infty}$).

The above equation is independent of microstructure and thus holds for all composite materials, provided effective medium theory can be applied. In Figure 6, we compare the measured values of $\Delta\varepsilon_{\text{eff}}$ to those calculated using (16) (inserting the experimental data for $\Delta\varepsilon_m$, $\varepsilon_{m,\infty}$, and $\varepsilon_{\text{eff},\infty}(f)$). The experimental values are up to 38% higher (at $f = 10\%$) compared to what we may expect. Note that (3) and thus (12) to (16) presuppose that there are only two phases and that their properties remain unchanged when the components are mixed. But obviously, this basic assumption of effective medium theory is not fulfilled here. There are two possibilities.

(i) According to (16), the measured relaxation strength is proportional to the intrinsic one, $\Delta\varepsilon_{\text{eff}} \propto \Delta\varepsilon_m/\varepsilon_{m,\infty}$. So we can understand the experimental result when we assume that the dispersion of particles alters the molecular polarizability of the polymer by enhancing the relaxation strength of the matrix compared to that of the bulk polymer. In fact, replacing, in (16),

$$\frac{\Delta\varepsilon_m}{\varepsilon_{m,\infty}} \longrightarrow \frac{\Delta\varepsilon_m}{\varepsilon_{m,\infty}} \cdot (1 + f \cdot 3.8) \tag{17}$$

allows us to describe satisfactorily well the experimental data. Such a process is possible at the interfaces between particles and the matrix, where the molecular interactions are altered (and possibly interphases form). The smaller the particles, the stronger the impact of the interfaces [38–40]. In this case, the additional increase of relaxation strength should be proportional to the surface area of the interfaces and thus proportional to f, what we in fact do observe (see Figure 6). Further experiments will show whether also the temperature dependence of the relaxation time is affected by these altered interactions.

(ii) Charge transfer between agglomerating particles, either via contact resistances (corresponding to a third phase in the mixture) or via a hopping process, can lead to an additional interfacial polarization process [23, 41]. The characteristic frequency of such a process is proportional to the conductivity of the polarized object. Attributing a conductivity $\sigma_{\text{aggl}} \ll \sigma_p$ to the agglomerates, it might be located in the low frequency range and, just by chance, coincide with that of the dipolar relaxation of the polymer matrix. We consider this implausible, especially since the measured data in Figures 3(b) and 4(b) does not indicate the appearance of a new distinct peak. But the form of the relaxation peak changes on addition of nanoparticles, so that we cannot completely exclude this hypothesis. But then the two mechanisms (dipolar relaxation and agglomerate polarization) should have different activation energies, so that future temperature dependent measurements should allow us to separate the respective loss peaks.

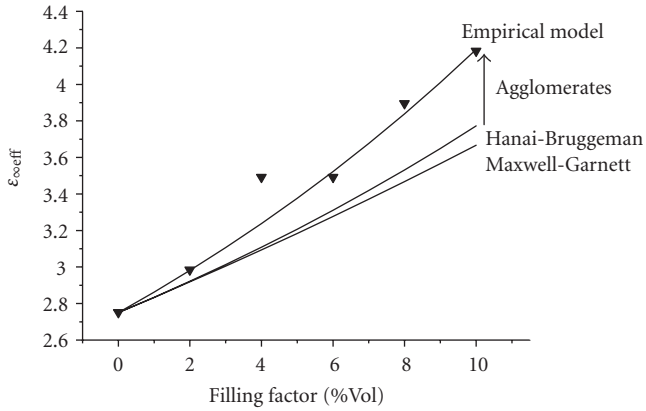

FIGURE 7: High-frequency permittivity versus volume filling factor. The solid lines correspond to the models of Maxwell-Garnett (13) and Hanai-Bruggeman (14) as well as to (18) (see text).

Now, let us focus on the high-frequency permittivity, $\varepsilon_{\text{eff},\infty}$, which is shown as a function of filling factor

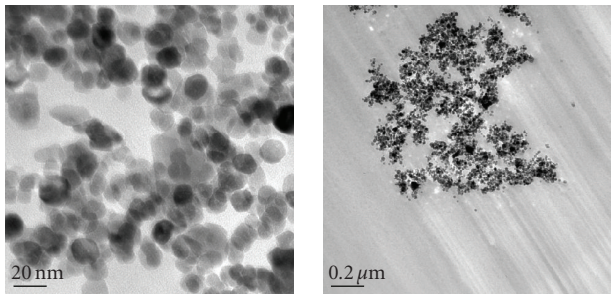

(a) (b)

Figure 8: TEM-pictures of a sample with $f = 2\%$. Note the different magnifications.

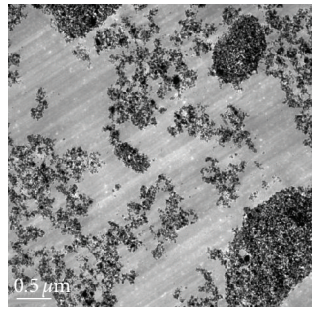

Figure 9: TEM-photo of a sample with $f = 10\%$.

in Figure 7. ε_∞ increases with f. We compare the experimental data with two models which apply for a statistical spatial distribution of spheres in a continuous matrix (matrix-inclusion topology or cermet topology). For monodisperse systems below the percolation threshold, the Maxwell-Garnett model applies, see (13), whereas the polydisperse limit (i.e., spheres with a sufficiently broad size distribution) is well described by the Hanai-Bruggeman model, see (14). These formulas and their range of application have been verified by 3D computer simulations based on an analytically exact solution [19, 20].

Obviously, both models predict permittivities that are lower than those measured. This deviation is nonambiguous since, in the quasistatic limit, the effective permittivity does not depend on an unknown particle permittivity, ε_p. But we can describe the experimental data fairly well by a modified version of the Hanai-Bruggeman model, see (14), where the exponent 3 is replaced by 4 (see Figure 7):

$$\varepsilon_{\text{eff},\infty}^{\text{exp}} \simeq \frac{\varepsilon_{m,\infty}}{(1-f)^4}. \tag{18}$$

This is just an empirical description, but it will facilitate the evaluation of the magnetic measurements (see below).

In order to find out to which extent the observed enhancement is related to the microstructure of our composite, transmission electronic microscopy measurements have been performed. In Figures 8 and 9, we show TEM-pictures of two samples. Agglomerates are clearly observable, that is, there is no random spatial distribution. This leads to a higher-effective permittivity compared to simple effective-medium

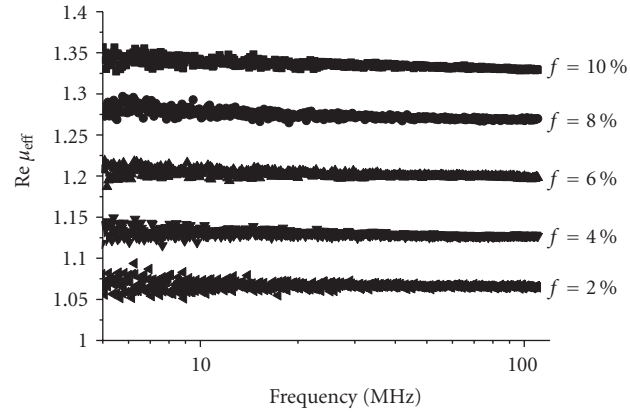

Figure 10: Real part of permeability versus frequency for samples with different volume filling factors. The imaginary part vanishes within the resolution of the measurement method.

models [23]. Of course, we cannot exclude that there is an additional effect, for example, an enhancement of the matrix permittivity, $\varepsilon_{m,\infty}$, due to altered interactions at the interfaces between matrix and nanoparticles, similar to what we have discussed above.

4. MAGNETIC MEASUREMENTS

Now, let us see what kind of information we can get from the magnetic measurements. These have been performed for the samples listed in Table 2. At low frequencies from 5 to 110 MHz, no losses can be observed ($\mu_{\text{eff}}'' \simeq 0$), so that we only display the real part of the effective permeability as a function of the frequency in Figure 10. The permeability increases by adding nanoparticles to our nonmagnetic matrix (see also Figure 12).

As already stated in the introduction, in the framework of effective medium theory, magnetic permeability is treated in the same way as permittivity, so that we can replace ε by μ in all formulas. But compared to the analysis of dielectric data, there are two differences in the discussion of magnetic measurements.

(i) We consider a nonmagnetic matrix, $\mu_m = 1$, and this property cannot change due to interface effects in the composite. This facilitates the analysis of the data.

(ii) The effective permeability will now depend not only on the microstructure, but also on the permeability of the dispersed particles, μ_p. Thus $\mu_{\text{eff}} = F(\mu_p, \mu_m, f)$ holds with an unknown function F. In addition, μ_p may differ from the bulk value and thus it is unknown as well. This makes an analysis more complicated.

So the question arises whether it is possible to determine μ_p although we do not dispose *a priori* of an analytical effective medium formula that is appropriate for the microstructure of our samples. For example, when we fit our data in Figure 10 using the Hanai-Bruggeman formula,

$$\left(\frac{\mu_{\text{eff}} - \mu_p}{\mu_m - \mu_p}\right) \cdot \left(\frac{\mu_m}{\mu_{\text{eff}}}\right)^{1/3} = (1-f), \tag{19}$$

we obtain a value of $\mu_p \simeq 40$ (see Figure 11). But remember that both the dielectric measurements and the TEM-pictures have shown that the particles are not randomly dispersed. Similar to what we have observed in the dielectric case, the formation of agglomerates partly contributes to the observed increase of effective permeability. This can be understood in terms of an enhanced particle interaction: in random systems, higher-multipole moments can be neglected [20], but they gain in importance in agglomerates. Therefore, the obtained value can only be considered as an upper limit, that is, we can expect $\mu_p < 40$. At first sight, it seems to be impossible to get a reliable value for μ_p without further information about the microstructure and an appropriate model to describe it. But in the following, we are going to show that the dielectric measurements described above give us all the structural information we need to evaluate the particle permeability. Instead of relying on approximate effective medium formulas, we can use the spectral representation, that is, an analytically exact formulation.

Although the spectral density, $g_f(n)$, is unknown, we have four sources of integral information to solve the problem: the two sum rules, (4) and (5), as well as the dielectric measurements in the quasistatic limit (Figure 7) and magnetic low frequency measurements (below 110 MHz, see Figure 12). Equations (6) and (12) relate the experimental data to the properties of the components and the spectral density. Using these and the above definition of the quasisatic dielectric limit, $h(f) = \lim_{|\varepsilon_p|\to\infty}(\varepsilon_{\text{eff}}/\varepsilon_m)$, we obtain

$$h(f) - \frac{\mu_{\text{eff}}(f)}{\mu_m} = \left(1 + f\int_0^1 \frac{g_f(n)}{n}dn\right) - \left(1 + f\int_0^1 \frac{g_f(n)}{t_\mu + n}dn\right) = f\int_0^1 \frac{g_f(n)}{n}\cdot\frac{t_\mu}{n+t_\mu}dn. \tag{20}$$

A Taylor expansion at $n = 1$ of the 2nd factor in the integral yields

$$\frac{t_\mu}{n+t_\mu} = \frac{t_\mu}{1+t_\mu} - \frac{t_\mu}{(1+t_\mu)^2}\cdot(n-1) + \frac{t_\mu}{(1+t_\mu)^3}\cdot(n-1)^2 - \frac{t_\mu}{(1+t_\mu)^4}\cdot(n-1)^3 + \cdots. \tag{21}$$

Inserting this result into (20) and performing the integration (using the sum rules (4) and (5) with $C = 0$), we obtain

$$\frac{\mu_{\text{eff}}(f)}{\mu_m} = h(f) - \frac{t_\mu}{1+t_\mu}\cdot(h(f)-1) - \frac{t_\mu}{(1+t_\mu)^2}\cdot[(h(f)-1) - f] - \frac{t_\mu}{(1+t_\mu)^3}\cdot\left[(h(f)-1) - 5/3\cdot f - 1/3\cdot f^2\right] + \cdots. \tag{22}$$

The known limiting cases are easily checked; for $\mu_p/\mu_m = 1$, that is, $t_\mu = \infty$, we obtain $\mu_{\text{eff}}/\mu_m = 1$. For $\mu_p/\mu_m \to \infty$, that is, $t_\mu \to 0$, we get once again the quasistatic limit $\mu_{\text{eff}}/\mu_m \to h(f)$. It can be easily shown that the next higher term of order $t_\mu/(1+t_\mu)^4$ in (22) contributes at maximum 1% of $h(f)$ and thus it can be neglected. The implications of the above result, that has been obtained using spectral density analysis, are obvious.

Equation (22) allows us to evaluate t_μ and thus the particle permeability μ_p. The only quantities we need to know are the effective permeability as well as the quasistatic dielectric limit, $h(f) = \lim_{|\varepsilon_p|\to\infty}(\varepsilon_{\text{eff}}/\varepsilon_m)$. One possibility would be to insert the measured values and to solve (22) for t_μ at the respective concentration f. But there is a better way that helps to minimize the influence of statistical measurement errors as well as that of structural variations or of concentration fluctuations (remember that different samples are used to determine ε_{eff} and μ_{eff}): when the particle concentration has been varied it is advantageous to use a simple fit function to describe the measured dielectric data. From our dielectric measurements, we know that $h(f) \simeq 1/(1-f)^4$ holds ((18) and Figure 7). Inserting this function in (22), we can directly calculate the effective permeability $\mu_{\text{eff}}(f)$ for different values of μ_p. In Figure 12, we compare this calculation with the measured low-frequency permeability. Obviously, the magnetite nanoparticles exhibit a permeability of

$$\mu_p = 7 \pm 1. \tag{23}$$

The advantage of the above evaluation procedure consists in the fact that (22) holds for an arbitrary microstructure. The only prerequisite is that the dispersed particles are conductive. In this case, a combination of dielectric and magnetic measurements enables us to determine the permeability of the dispersed particles without using any effective medium model!

At high frequencies from 110 MHz to 6 GHz, we have performed reflection measurements. The effective permeability is shown as a function of the frequency in Figure 13. Near 3 GHz, a ferromagnetic resonance can be observed. The strength of this process increases with the addition of nanoparticles, but the resonance frequency seems not to depend on the particle concentration. That is what also theoretical models predict for single-domain particles with an isotropic distribution of magnetic orientations [42]. So the situation is quite different from what is known for dielectric relaxation in dispersed particles, where the phase shift of the electric field at the interfaces induces a shift of the measurable effective relaxation frequency compared to that of the intrinsic relaxation [24]: when a complex relaxation function, $\varepsilon_p(\nu)$, is inserted into (1) or (3), the position of the effective loss peak is shifted to higher frequencies (an effect that depends on filling factor and microstructure). But note that, in the present case of ferromagnetic resonance, effective medium theory does not apply in its scalar form, even though the effective permeability of single-domain particles with an isotropic distribution of magnetic orientations is a scalar quantity [42]; close to the resonance frequency, the particle permeability is a tensor, the nondiagonal components of which do not vanish. This makes the calculation

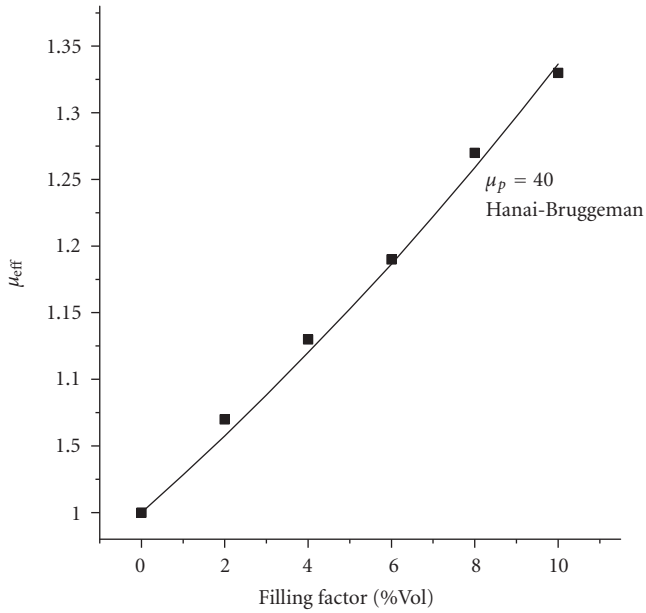

FIGURE 11: Effective permeability as a function of volume filling factor f. Symbols: experimental data (plateau values from Figure 10, i.e., at frequencies below 110 MHz). The solid line corresponds to the Hanai-Bruggeman formula, see (19), with $\mu_p = 40$ and $\mu_m = 1$. However, the dielectric data of Figure 7 shows that this model is not appropriate.

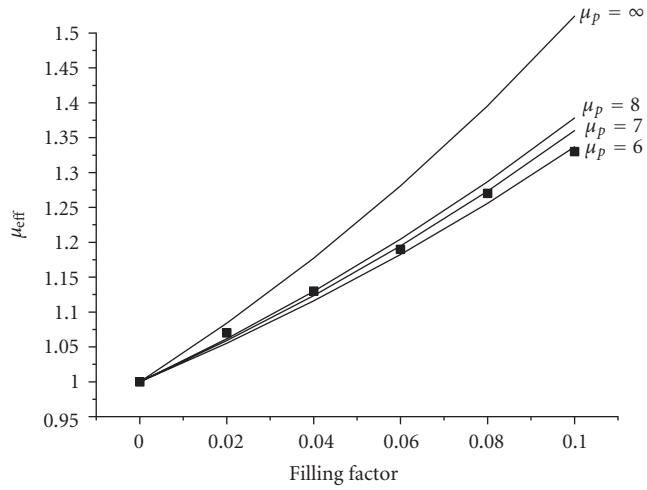

FIGURE 12: Effective permeability as a function of volume filling factor f. Symbols: experimental data (plateau values from Figure 10, i.e., at frequencies below 110 MHz). The solid lines correspond to (22) with $\mu_m = 1$ and the specified values of μ_p.

of μ_{eff} much more complicated and simple effective medium formulas should be handled with care.

5. CONCLUSION

We have prepared magnetic nanocomposites and we characterized them using broadband dielectric and magnetic spectroscopy. The dispersed particles (magnetite) are conductive, so that the dielectric data corresponds to the quasistatic limit of completely polarized particles. This leads to an enhancement of permittivity that is higher than what can be expected for a spatial random distribution of particles. In fact, TEM-pictures show the presence of particle agglomerates. Moreover, the addition of nanoparticles alters the molecular dynamics of the matrix polymer at low frequencies. This effect is due to the modified interactions at the interfaces between particles and the matrix. The measured effective permeability depends both on the microstructure and on the permeability of the nanoparticles, μ_p. We have proposed a model-free procedure, that allows us to evaluate μ_p without using effective medium formulas. It applies for an arbitrary and possibly unknown microstructure and consists of combining dielectric and magnetic data using the spectral representation. In this way, we have determined a value of $\mu_p = 7 \pm 1$ for the permeability of the dispersed magnetite. At high frequencies, the ferromagnetic resonance of the nanoparticles is observed. It is independent of particle concentration and occurs near 3 GHz.

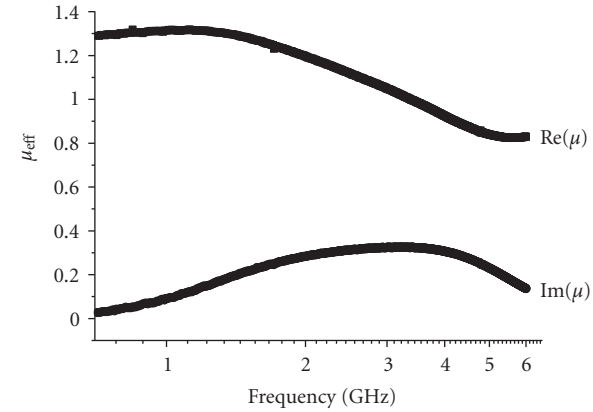

(a)

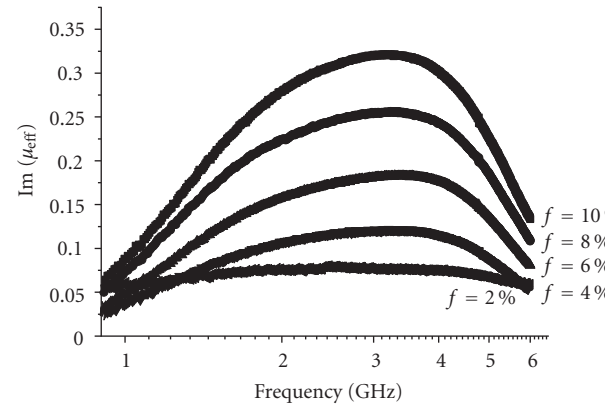

(b)

FIGURE 13: (a) Measured real and imaginary part of permeability as a function of frequency for a sample with $f = 10\%$. (b) Measured imaginary part of permeability for samples with various filling factors. Near 3 GHz, the ferromagnetic resonance is observed.

ACKNOWLEDGMENT

The authors gratefully acknowledge the help of J. Schmauch (Universität des Saarlandes), who took the TEM-pictures of our samples.

REFERENCES

[1] R. Ramprasad, P. Zurcher, M. Petras, M. Miller, and P. Renaud, "Magnetic properties of metallic ferromagnetic nanoparticle composites," *Journal of Applied Physics*, vol. 96, no. 1, pp. 519–529, 2004.

[2] M. Dikeakos, L. D. Tung, T. Veres, A. Stancu, L. Spinu, and F. Normandin, "Fabrication and characterization of tunable magnetic nanocomposite materials," *Materials Research Society Symposium Proceedings*, vol. 734, no. 134, pp. 315–320, 2003.

[3] V. B. Bregar, "Advantages of ferromagnetic nanoparticle composites in microwave absorbers," *IEEE Transactions on Magnetics*, vol. 40, no. 3, pp. 1679–1684, 2004.

[4] J. Monecke, "Microstructure dependence of material properties of composites," *Physica Status Solidi (B)*, vol. 154, no. 2, pp. 805–813, 1989.

[5] G. Bánhegyi, "Comparison of electrical mixture rules for composites," *Colloid & Polymer Science*, vol. 264, no. 12, pp. 1030–1050, 1986.

[6] K. Günther and D. Heinrich, "Dielektrizitätskonstante, Permeabilität, elektrische Leitfähigkeit, Wärmeleitfähigkeit und Diffusionskonstante von Gemischen mit kugelförmigen Teilchen (gitterförmige und statistische Anordnung," *Zeitschrift für Physik*, vol. 185, no. 4, pp. 345–374, 1965.

[7] D. R. McKenzie, R. C. McPhedran, and G. H. Derrick, "The conductivity of lattices of spheres. II. The body centred and face centred cubic lattices," *Proceedings of the Royal Society of London. Series A*, vol. 362, no. 1709, pp. 211–232, 1978.

[8] N. Harfield, "Conductivity of a periodic particle composite with spheroidal inclusions," *The European Physical Journal—Applied Physics*, vol. 6, no. 1, pp. 13–21, 1999.

[9] N. Harfield, "Bulk permittivity of a composite with coated spheroidal filler particles," *Journal of Materials Science*, vol. 35, no. 23, pp. 5809–5816, 2000.

[10] S. Stölzle, A. Enders, and G. Nimtz, "Numerical simulation of random composite dielectrics," *Journal de Physique I*, vol. 2, pp. 401–408, 1992.

[11] S. Stölzle, A. Enders, and G. Nimtz, "Numerical simulation of random composite dielectrics. II. Simulations including dissipation," *Journal de Physique I*, vol. 2, pp. 1765–1777, 1992.

[12] H. Leinders and A. Enders, "Computer simulations of dielectric and magnetic composite media including dissipation," *Journal de Physique I*, vol. 5, pp. 555–564, 1995.

[13] E. Tuncer, "On complex permittivity of dilute random binary dielectric mixtures in two-dimensions," *Turkish Journal of Physics*, vol. 27, no. 2, pp. 101–105, 2003.

[14] E. Tuncer, B. Nettelblad, and S. M. Gubanski, "Non-Debye dielectric relaxation in binary dielectric mixtures (50-50): randomness and regularity in mixture topology," *Journal of Applied Physics*, vol. 92, no. 8, pp. 4612–4624, 2002.

[15] C. Brosseau and A. Beroual, "Computational electromagnetics and the rational design of new dielectric heterostructures," *Progress in Materials Science*, vol. 48, no. 5, pp. 373–456, 2003.

[16] C. Brosseau and A. Beroual, "Dielectric properties of periodic heterostructures: a computational electrostatics approach," *The European Physical Journal—Applied Physics*, vol. 6, pp. 23–31, 1999.

[17] V. Myroshnychenko and C. Brosseau, "Finite-element method for calculation of the effective permittivity of random inhomogeneous media," *Physical Review E*, vol. 71, no. 1, Article ID 016701, 16 pages, 2005.

[18] F. Wu and K. W. Whites, "Quasi-static effective permittivity of periodic compositescontaining complex shaped dielectric particles," *IEEE Transactions on Antennas and Propagations*, vol. 49, no. 8, pp. 1174–1182, 2001.

[19] L. Fu, P. M. Macedo, and L. Resca, "Analytic approach to the interfacial polarization of heterogeneous systems," *Physical Review B*, vol. 47, no. 20, pp. 13818–13829, 1993.

[20] A. Spanoudaki and R. Pelster, "Effective dielectric properties of composite materials: the dependence on the particle size distribution," *Physical Review B*, vol. 64, no. 6, Article ID 064205, 6 pages, 2001.

[21] L. K. H. van Beek, "Dielectric behaviour of heterogeneous systems," in *Progress in Dielectrics*, J. B. Birks, Ed., vol. 7, pp. 69–114, Heywood, London, UK, 1967.

[22] S. S. Dukhin, "Dielectric properties of disperse systems," in *Surface and Colloid Science*, E. Matijevic, Ed., vol. 3, pp. 83–165, Wiley-Interscience, New York, NY, USA, 1986.

[23] R. Pelster and U. Simon, "Nanodispersions of conducting particles: preparation, microstructure and dielectric properties," *Colloid & Polymer Science*, vol. 277, no. 1, pp. 2–14, 1999.

[24] R. Pelster, "Dielectric spectroscopy of confinement effects in polar materials," *Physical Review B*, vol. 59, no. 14, pp. 9214–9228, 1999.

[25] V. M. Shalaev, "Electromagnetic properties of small-particle composites," *Physics Reports*, vol. 272, no. 2-3, pp. 61–137, 1996.

[26] D. J. Bergman, "The dielectric constant of a composite material—a problem in classical physics," *Physics Reports*, vol. 43, no. 9, pp. 377–407, 1978.

[27] D. Stoud, G. W. Milton, and B. R. De, "Analytical model for the dielectric response of brine-saturated rocks," *Physical Review B*, vol. 34, no. 8, pp. 5145–5153, 1986.

[28] A. V. Osipov, K. N. Rozanov, N. A. Simonov, and S. N. Starostenko, "Reconstruction of intrinsic parameters of a composite from the measured frequency dependence of permeability," *Journal of Physics: Condensed Matter*, vol. 14, no. 41, pp. 9507–9523, 2002.

[29] E. Tuncer, N. Bowler, and I. J. Youngs, "Application of the spectral density function method to a composite system," *Physica B*, vol. 373, no. 2, pp. 306–312, 2006.

[30] C. Pecharromán and F. J. Gordillo-Vázquez, "Expansion of the spectral representation function of a composite material in a basis of legendre polynomials: experimental determination and analytic approximations," *Physical Review B*, vol. 74, Article ID 035120, 10 pages, 2006.

[31] B. Hallouet, "Simulationen und experimentelle Untersuchungen der dielektrischen und magnetischen Eigenschaften von Nanokompositen," Diploma thesis, Universität des Saarlandes, Saarbrücken, Germany, 2006.

[32] R. Pelster, "A novel analytic method for the broadband determination ofelectromagnetic impedances and material parameters," *IEEE Transactions on Microwave Theory and Techniques*, vol. 43, no. 7, pp. 1494–1501, 1995.

[33] Agilent Technologies, "Agilent 16454A Magnetic Material Test Fixture Operation and Service Manual," Agilent Part no. 16454-90020, Fifth Edition, July 2001.

[34] J. Kanzow, P. Schulze Horn, M. Kirschmann, et al., "Formation of a metal/epoxy resin interface," *Applied Surface Science*, vol. 239, no. 2, pp. 227–236, 2005.

[35] S. Havriliak and S. Negami, "A complex plane analysis of alpha-dispersions in some polymer systems," *Journal of Polymer Science Part C*, pp. 14–99, 1966.

[36] C. J. F. Böttcher and P. Bordewijk, *Theory of Electric Polarization: Dielectrics in Time-Dependent Fields*, vol. 2, Elsevier, Amsterdam, The Netherlands, 1978.

[37] S. P. Sena, R. A. Lindley, H. J. Blythe, Ch. Sauer, M. Al-Kafarji, and G. A. Gehring, "Investigation of magnetite thin films produced by pulsed laser deposition," *Journal of Magnetism and Magnetic Materials*, vol. 176, no. 2, pp. 111–126, 1997.

[38] T. J. Lewis, "Interfaces: nanometric dielectrics," *Journal of Physics D*, vol. 38, no. 2, pp. 202–212, 2005.

[39] T. J. Lewis, "Interfaces are the dominant feature of dielectrics at the nanometric level," *IEEE Transactions on Dielectrics and Electrical Insulation*, vol. 11, no. 5, pp. 739–753, 2004.

[40] J. K. Nelson and Y. Hu, "Nanocomposite dielectrics—properties and implications," *Journal of Physics D*, vol. 38, no. 2, pp. 213–222, 2005.

[41] R. Pelster, A. Spanoudaki, and T. Kruse, "Microstructure and effective properties of nanocomposites: ferrofluids as tunable model systems," *Journal of Physics D*, vol. 37, no. 3, pp. 307–317, 2004.

[42] V. B. Bregar, "Effective-medium approach to the magnetic susceptibility of composites with ferromagnetic inclusions," *Physical Review B*, vol. 71, no. 17, Article ID 174418, 8 pages, 2005.